Induced Current Due to Electromagnetic Shock Produced by Charge Impact on a Conducting Surface

Dion Li, *Student Member, IEEE*, Patrick Y. Wong, *Member, IEEE*, David Chernin, and Y. Y. Lau, *Fellow, IEEE*

***Abstract*— This article compares the transient induced current due to the electromagnetic shock produced by a charged particle impacting a perfectly conducting plate, with the classical, quasi-static induced current of Ramo and Shockley (RS). We consider the simple model of a line charge, removed upon striking the plate. We find that the induced current due to the shock is negligible compared with the RS current for nonrelativistic impact energies, but is more significant as the impact energy becomes mildly relativistic. The implications of these findings are discussed.**

***Index Terms*— Crossed-field devices, induced current, multipactor discharge, Ramo's Theorem, Ramo–Shockley Theorem.**

I. Introduction

THE classical Ramo–Shockley (RS) theorem gives the current induced on perfect conductors by the motion of nearby charges, assuming nonrelativistic motion of those charges in electrostatic fields [1], [2]. The RS theorem has been used with great success in vacuum electronics to approximate the radio-frequency (RF) beam current that drives traveling wave tubes, klystrons, and crossed-field devices [3]–[6]. It has also been used in the theory of multipactor discharge, to analyze its effects on the beam loading of RF circuits [7] and the degradation in signal quality [8]. We recently suggested the reasons for such successes, having extended the RS theory to include electromagnetic and relativistic effects, for the first time [9]. We obtained an exact, closed-form analytic solution for the induced current of a simple model of a line charge moving between two parallel plates and compared that solution with the classical RS value. The classical RS approach does not account for electromagnetic transients and multiple reflections, but otherwise works quite well even at relativistic velocities, before the electron line charge strikes and is removed by a conducting surface, at which time an electromagnetic shock is generated. This shock, a form of transition radiation [10], is completely absent from the electrostatic theory of RS. Note that the classical RS theory gives a zero value of the induced current at the instant of impact and thereafter. Thus, the additional beam loading due to the impact of electrons was omitted in all previous analyses of beam loading that made use of the classical RS. This shock-induced current was not included in the models of Kishek and Lau [7] and Chernin [6], who used the classical RS theory for the induced current to treat multipactor discharge and crossed-field amplifiers, respectively. This article addresses this issue by comparing the magnitude of the induced current produced by the transient electromagnetic shock due to the disappearance of a charge upon impact on a perfectly conducting plate, with the classical induced current according to RS.

In this article, we will continue to use the simple model of a line charge [9] moving between two parallel conducting plates of separation d [see Fig. 1(a)]. We will further assume that an AC voltage V_{RF} of frequency ω is imposed across the

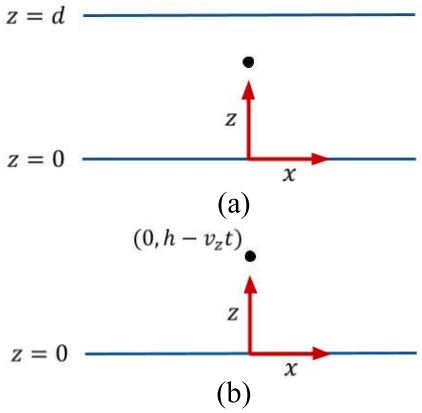

Fig. 1. (a) Parallel-plate model used to assess the electrostatic induced current. A sinusoidal steady-state voltage is imposed across the plates. (b) Single-plate model used to assess the shock-induced current. The line charge lies at $(x, z) = (0, h)$ initially. At $t = 0$, the charge experiences an impulse, downward acceleration to a velocity v_z. We shall later take $h \to \infty$, $T = h/v_z \to \infty$, and $t \to \infty$, with $(t - T)$ finite, to isolate the shock-induced current.

Manuscript received 3 March 2022; revised 30 May 2022; accepted 25 June 2022. Date of publication 21 July 2022; date of current version 23 September 2022. This work was supported in part by the Air Force Office of Scientific Research (AFOSR) under Grant FA9550-18-1-0153, Grant FA9550-18-1-0062, Grant FA9550-20-1-0409, and Grant FA9550-21-1-0367; and in part by the L3Harris Electron Devices Division. The review of this article was arranged by Senior Editor J. G. Leopold. *(Corresponding author: Y. Y. Lau.)*

Dion Li and Y. Y. Lau are with the Department of Nuclear Engineering and Radiological Sciences, University of Michigan, Ann Arbor, MI 48109 USA (e-mail: yylau@umich.edu).

Patrick Y. Wong was with the Department of Electrical and Computer Engineering, Michigan State University, East Lansing, MI 48824 USA.

David Chernin is with Leidos Inc., Reston, VA 20190 USA.

Color versions of one or more figures in this article are available at https://doi.org/10.1109/TPS.2022.3187667.

Digital Object Identifier 10.1109/TPS.2022.3187667

parallel plates and we use the classical RS theory to calculate the induced current due to the motion of the line charge within the plates during its transit, that is, before the line charge strikes a plate. We assume that the line charge motion is subject only to the vacuum AC electric field, ignoring the additional electrostatic field due to the image charges [7], [11]. We consider only the motion of the line charge in one transit, from one plate to the opposite plate, with a transit time $T = \pi/\omega$ exactly equal to 1/2 of the RF period. This assumption is consistent with the sinusoidal steady-state assumption, where an identical trip is repeated every cycle. The classical induced current according to RS during this single transit may then be calculated. When the line charge hits a plate, it is removed, and the classical RS-induced current is identically zero. To assess the electromagnetic shock-induced current due to the impact of the line charge at the terminal velocity v_z, we consider a separate, reduced problem in which we assume a single plate geometry, $d \to \infty$ [see Fig. 1(b)]. We assume that the line charge starts at a large distance from this single plate and it moves toward this plate at the constant terminal velocity, v_z, which is set equal to the impact velocity in the parallel-plate model. This line charge hits the single plate and is instantaneously removed. The shock-induced solution in this single plate problem may then be extracted from our exact solutions previously obtained. We find that this shock-induced current, when compared with the classical RS-induced current during transit (see Fig. 4 below), is relatively unimportant when $\beta = v_z/c$ is small, but becomes significant as β increases. These findings suggest that the electromagnetic shock would not significantly worsen the signal quality in a multipactor discharge, an important issue for satellite communication, but it could affect the beam loading in a relativistic magnetron or a magnetically insulated line oscillator (MILO). We shall further discuss these issues in Section III.

Section II presents the calculation of the electromagnetic, shock-induced current in a single-plate geometry, assuming that a line charge approaches this plate at a constant speed v_z from a faraway distance, using the model in Fig. 1(b). A calculation of the electrostatic-induced current during the transit of a line charge that moves between two parallel plates that is subjected to the sinusoidal gap voltage, V_{RF}, using the model in Fig. 1(a), is given in Section III. This electrostatic-induced current is compared with the shock-induced current calculated in Section II, assuming an identical impact velocity v_z. We also discuss the implications of this comparison. Section IV provides a summary and some additional observations.

II. Shock-Induced Current in the Single-Plate Geometry

In this section, we evaluate the shock-induced current when a line charge of charge density (λ, in C/m) strikes a perfectly conducting plate with a velocity v_z and is removed from the surface on impact. To avoid the complexities of multiple reflections of the electromagnetic waves, we consider the single-plate geometry of Fig. 1(b). We assume that the line charge is initially at rest and is located at $(x, z) = (0, h)$, as shown in Fig. 1(b). At $t = 0$, an impulse acceleration of the line charge is applied, so that the line charge moves downward at a constant velocity $-v_z$, striking the single plate at time $t = T = h/v_z$. For $0 < t < T$, the induced current on the conducting plate is due to the impulse acceleration at $t = 0$, and to the re-arrangements of the surface charge as a result of the constant downward motion of the line charge. The exact expression for the induced current on the conducting plate, $K_x = K_x(x, t)$, is given by [9, eq. (8)]

$$K_x = \frac{\lambda\gamma^2 v_z x}{\pi[x^2 + \gamma^2(h - v_z t)^2]} \times \frac{ct - hv_z/c}{[(ct)^2 - x^2 - h^2]^{1/2}}, \quad t < T \tag{1}$$

where we have replaced $v_z \to -v_z$ with $v_z > 0$. In (1), $\gamma = (1 - \beta^2)^{-1/2}$, $\beta = v_z/c$, and c is the speed of light.

To extract the shock-induced solutions, we need to eliminate the transient component and pay special attention to the solution in the vicinity of $t = T$. This may be accomplished by defining $t' = t - T$ and taking the limit of $t, T \to \infty$, while t' is finite. Physically, we assume $h \to \infty$ so that when the line charge hits the plate, the transient solution due to the impulse acceleration disappears. We then obtain (see Appendix A)

$$\bar{K}_x = \frac{\gamma\bar{x}}{\pi[\bar{x}^2 + \gamma^2\bar{t}'^2]} \tag{2}$$

for $t' < 0$. We have defined the dimensionless quantities $\bar{x} = x/L$, $\bar{t} = v_z t/L$, and $\bar{K} = K/(\lambda v_z/L)$, where L is an arbitrary scale length.

We next consider the induced current for all time, including $t \geq T$, after the line charge strikes the conducting plate and is removed instantaneously. In this case, the induced current may be derived from [9, Eq. (14)], which may be written, upon taking the single-plate limit ($n = 0$) and, once again, taking $\bar{h}, \bar{t} \to \infty$, while $\bar{t}'$ is finite (see Appendix B)

$$\bar{K}_x = \begin{cases} \dfrac{\gamma\bar{x}}{\pi[\bar{x}^2 + \gamma^2\bar{t}'^2]}, & \bar{t}' < 0 \quad \text{(3a)} \\ \dfrac{\gamma\bar{x}}{\pi[\bar{x}^2 + \gamma^2\bar{t}'^2]}\left\{1 - \dfrac{\gamma\bar{t}'/\beta}{[(\bar{t}'/\beta)^2 - \bar{x}^2]^{1/2}}\right\}, & \bar{t}' \geq 0 \quad \text{(3b)} \end{cases}$$

where we note that (3a) is identical to (2). It is straightforward to show that in the quasi-static limit, or when $c \to \infty$ or $\gamma \to 1$, (3) reduces to the classical RS result

$$\bar{K}_x^{\mathrm{ES}} = \begin{cases} \dfrac{\bar{x}}{\pi[\bar{x}^2 + \bar{t}'^2]}, & \bar{t}' < 0 \\ 0, & \bar{t}' \geq 0 \end{cases} \tag{4}$$

where the superscript ES stands for "electrostatic."

Since we are only interested in the induced current due to the electromagnetic shock produced by the line charge striking the conducting plate, we may modify (3) to be nonzero strictly within the "shock cone," $|x| < c(t - T)$, of the radiation produced by the impacting line charge. This allows us to write the induced current due exclusively to the shock, ignoring all transients (and all electromagnetic wave reflections for the case

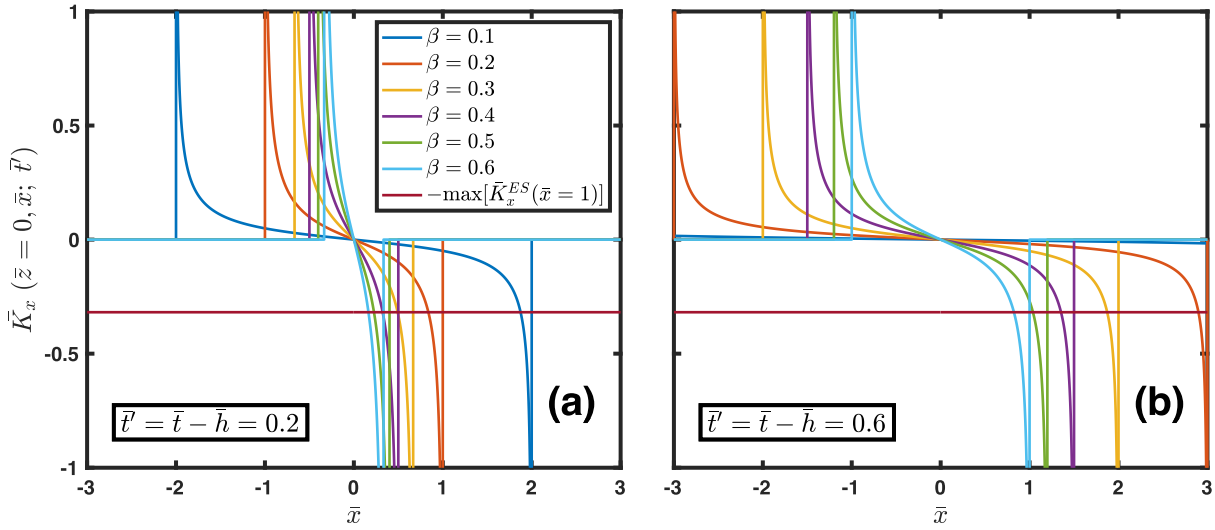

Fig. 2. Shock-induced currents, $\bar{K}_x^{\mathrm{SH}}$ [see (5)] at $\bar{x} = 1$ evaluated at (a) $\bar{t}' = \bar{t} - \bar{h} = 0.2$ and (b) $\bar{t}' = 0.6$ with six different β values. Also plotted for reference is -1 times the maximum value of the classical RS-induced current $\bar{K}_x^{\mathrm{ES}}(\bar{x} = 1)$.

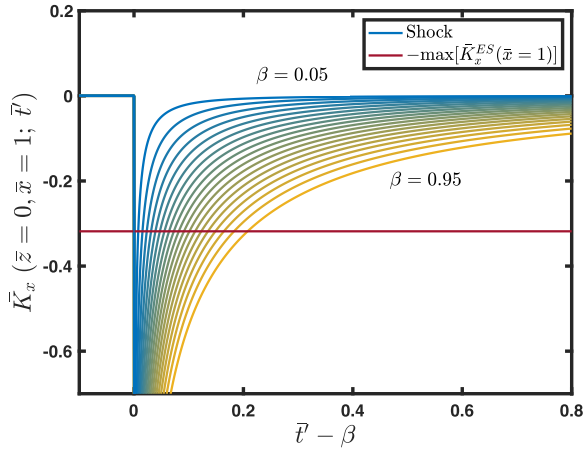

Fig. 3. Time evolution of the shock-induced currents, $\bar{K}_x^{\mathrm{SH}}$ [see (5)], evaluated at $\bar{x} = 1$ on the single plate at $z = 0$, due to an impacting line charge for 19 different values of β ($\beta = 0.05, 0.1, \ldots, 0.95$), compared with the reference electrostatic-induced current value $1/\pi$. Note that the blue curves correspond to lower (less relativistic) impact velocities and the yellow curves correspond to higher (more relativistic) impact velocities.

of a parallel plate geometry)

$$\bar{K}_x = \bar{K}_x^{\mathrm{SH}} = \begin{cases} \dfrac{\gamma\,\bar{x}}{\pi\,[\bar{x}^2 + \gamma^2 \bar{t}'^2]} \left\{ 1 - \dfrac{\gamma\,\bar{t}'/\beta}{[(\bar{t}'/\beta)^2 - \bar{x}^2]^{1/2}} \right\}, \\ \qquad \bar{t}' > |\beta \bar{x}| \\ 0, \quad \text{otherwise} \end{cases} \tag{5}$$

where the superscript SH stands for "shock-induced." Clearly, $\bar{K}_x^{\mathrm{ES}} = 0$ when $\bar{t}' > |\beta \bar{x}|$ according to (4).

As a sense of scale for the magnitude of the quasistatic-induced current, we compare the maximum value of $\bar{K}_x^{\mathrm{ES}}$ at $\bar{x} = 1$ with $\bar{K}_x^{\mathrm{SH}}$, noting that $\bar{K}_x^{\mathrm{ES}}(\bar{x} = 1)$ is largest when $\bar{t}' = 0$ [cf. (4)], taking on the value $\bar{K}_x^{\mathrm{ES}} = 1/\pi$. The exact induced current at multiple values of β are plotted with -1 times the reference value $1/\pi$ in Fig. 2. Fig. 3 illustrates how the impact velocity of the line charge affects the time evolution of the shock-induced current. As with Fig. 2, the reference value of $-1/\pi$ is overlaid.

It appears that the "widths" of the normalized shock-induced current curves, $\bar{K}_x^{\mathrm{SH}}$ versus $\bar{t}'$ (see Fig. 3), are narrower for less relativistic velocities and wider for more relativistic velocities. In the limit $\beta \to 0$, the shock-induced current curve becomes infinitely narrow. Regardless of β, the shock-induced surface current approaches $\bar{K}_x^{\mathrm{SH}} \to -\infty$ at $\bar{t}' - \beta = 0$. However, it appears that for deeply nonrelativistic impact velocities, corresponding to hundreds of eV or less such as those associated with the participating electrons in a multipactor discharge [7], the shock-induced current would have a negligible influence, compared with the induced current during transit that is described by the classical RS. This comparison is given in Section III.

III. Comparison With the Classical Induced Current in a Parallel-Plate Geometry

For the induced current according to the classical RS theory, we use the parallel plate model [see Fig. 1(a)] and assume that the potential at the lower plate is zero and at the upper plate is $V_{\mathrm{RF}} = \tilde{V}_{\mathrm{RF}} \sin(\omega t_1 + \theta)$, where the electron line charge is initialized at $t_1 = 0$ somewhere within the plates. We shall consider only the classical electrostatic induced current during transit, that is, before this electron strikes a plate. If the initial position of the line charge is at the upper plate, and if it reaches the lower plate after half an RF cycle (i.e., the transit time $\tau = \pi/\omega$), this is equivalent to the model of a two-surface steady-state multipactor discharge of order one [7], [11]. There is a "phase-locking condition" on the sinusoidal steady state. Assuming nonrelativistic voltage and ignoring space charge effects, this condition reads [11]

$$\tilde{V}_{\mathrm{RF}} = \frac{md^2}{e} \frac{\omega^2 \left(1 - \frac{\pi v_0}{\omega d}\right)}{2 \sin\theta + \pi \cos\theta} \tag{6}$$

where $\tilde{V}_{\mathrm{RF}}$ is the amplitude of the RF voltage, θ is the "launch phase," and v_0 is the initial velocity of the line charge. Setting

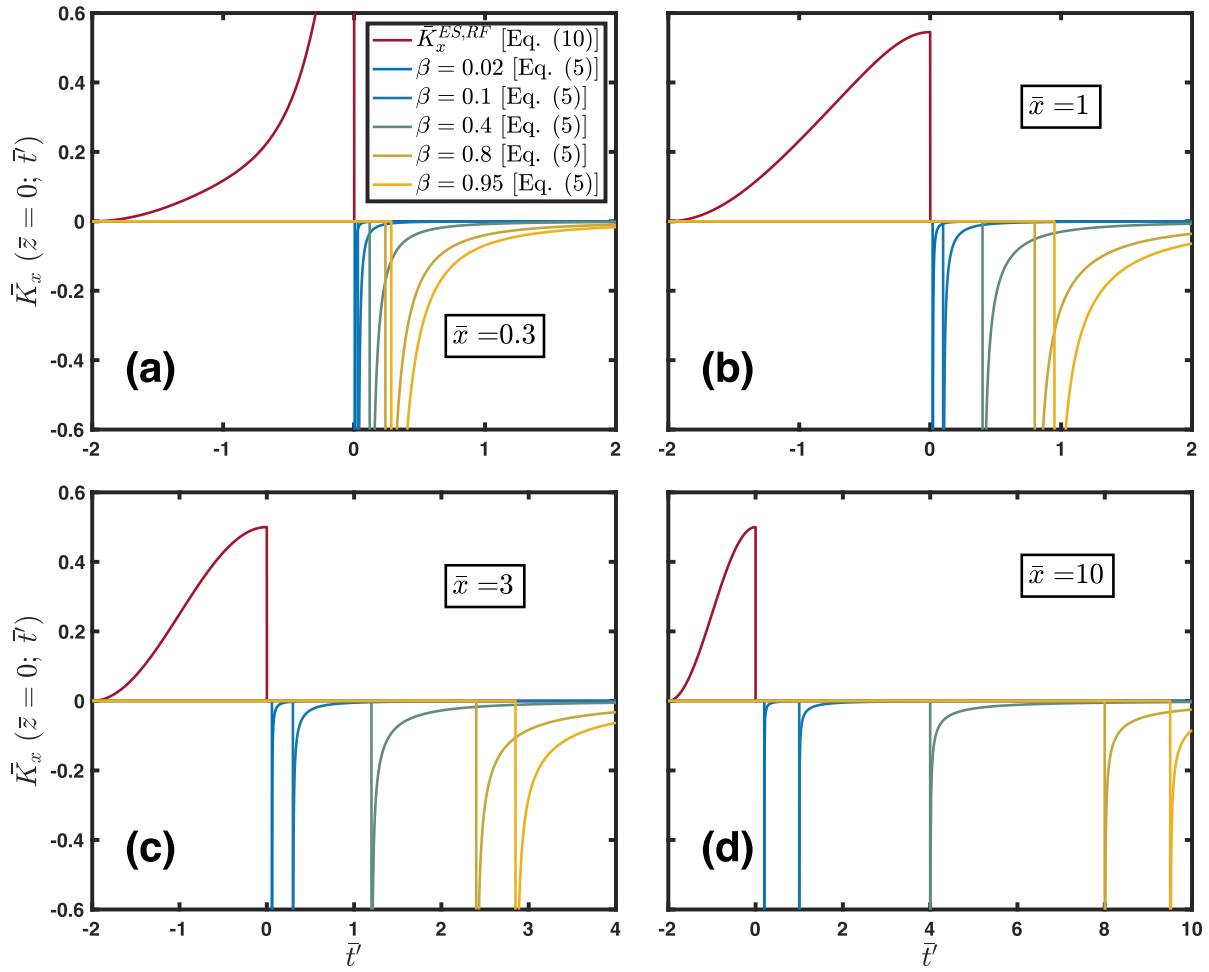

Fig. 4. Time evolution of the normalized electrostatic, parallel-plate-induced current from a line charge subject to an RF electric field [see (10)], compared with the normalized induced currents due to the electromagnetic shock of the impacting line charge [see (5)] at $\bar{x}$ = (a) 0.3, (b) 1.0, (c) 3.0, and (d) 10. Five different values of β were used, $\beta = 0.02$, 0.1, 0.4, 0.8, and 0.95, corresponding to impact energies of, respectively, 0.102, 2.574, 46.54, 340.7, and 1126 keV. The normalized electrostatic induced current exists only for $\bar{t}' < 0$ and is independent of the gap voltage (or β) in the present model. The shock-induced current exists only for $\bar{t}' \geq 0$.

$v_0 = 0$ and $\theta = \pi$, $\tilde{V}_{\rm RF}$ has a magnitude

$$\tilde{V}_{\rm RF} = \frac{md^2\omega^2}{\pi e}. \tag{7}$$

We next solve for $z(t_1)$ and $\dot{z}(t_1)$ from the nonrelativistic force law within the parallel plates [see Fig. 1(a)] to obtain

$$z(t_1) = d - \frac{d}{\pi}(\omega t_1 - \sin\omega t_1) \tag{8a}$$

$$\dot{z}(t_1) = -\frac{\omega d}{\pi}(1 - \cos\omega t_1) \tag{8b}$$

so that $z(0) = d$ and $\dot{z}(0) = 0$. In the quasistatic regime, the classical (RS) induced current on the lower plate is [9]

$$K_x^{\rm ES,RF} = -\frac{\lambda\dot{z}(t_1)}{2d}\frac{\sinh\left(\frac{x\pi}{d}\right)}{\cosh\left(\frac{x\pi}{d}\right) - \cos\left(\frac{\pi}{d}z(t_1)\right)} = \frac{\lambda\omega}{2\pi}\frac{(1-\cos\omega t_1)\sinh\left(\frac{x\pi}{d}\right)}{\cosh\left(\frac{x\pi}{d}\right) - \cos\left(\frac{\pi}{d}\left(d - \frac{d}{\pi}(\omega t_1 - \sin\omega t_1)\right)\right)} \tag{9}$$

where $0 < t_1 < \tau$ and $\tau = \pi/\omega$ is the transit time of the line charge. Since we have previously set the magnitude of the impact velocity as the velocity scale, v_z, let us do the same here. We thus obtain $\dot{z}(t_1 = \pi/\omega) = -2\omega d/\pi = -v_z$, and similarly nondimensionalize $\bar{t}_1 = 2\omega t_1/\pi$ and $\bar{K} = K/(2\lambda\omega/\pi)$. The normalized classical induced current becomes

$$\bar{K}_x^{\rm ES,RF} = \begin{cases} \dfrac{1}{4}\dfrac{\left(1-\cos\left(\frac{\pi}{2}(\bar{t}'+2)\right)\right)\sinh(\pi\bar{x})}{\cosh(\pi\bar{x}) - \cos\left(-\frac{\pi}{2}\bar{t}' + \sin\left(\frac{\pi}{2}(\bar{t}'+2)\right)\right)}, \\ \qquad -2 < \bar{t}' < 0 \\ 0, \quad \text{otherwise} \end{cases} \tag{10}$$

where $\bar{t}' = \bar{t}_1 - \bar{\tau} = \bar{t}_1 - 2$. Note that (10) is independent of $\tilde{V}_{\rm RF}$ and ω. This enables a convenient comparison between this classical induced current during transit and the shock-induced current. The shock-induced current depends on $\tilde{V}_{\rm RF}$, which determines the impact velocity, $v_z = \beta c$, the velocity assumed in the model in Section II. Fig. 4 overlays (10) with (5), taking on multiple β values. Each β value corresponds to a unique ω and, therefore, a unique $\tilde{V}_{\rm RF}$ by $\omega = \pi c\beta/2d$ and $\tilde{V}_{\rm RF} = \pi mc^2\beta^2/4e$, respectively, in the nonrelativistic case. In Fig. 4, the induced current during transit ($\bar{t}' < 0$) reverses its sign

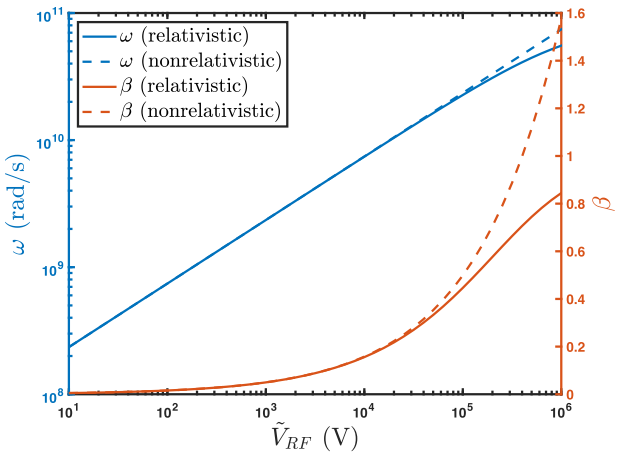

Fig. 5. Comparison of ω and β as a function of $\tilde{V}_{\mathrm{RF}}$ in the nonrelativistic (dashed curves) and relativistic (solid curves) regimes with gap spacing $d = 0.01$ m.

after impact ($\bar{t}' > 0$), because in the former case, an image charge is being added to the plate, whereas in the latter case, an image charge is removed from the plate.

The analysis in this section has thus far assumed nonrelativistic electron motion. An extension to relativistic motion using the same sinusoidal AC gap voltage is given in Appendix C. Comparisons of the nonrelativistic and relativistic values of ω and β as a function of $\tilde{V}_{\mathrm{RF}}$ are shown in Fig. 5.

It is important to note that the comparison in Fig. 4 has ignored the multiple reflections which necessarily occur in the parallel plate model in a fully electromagnetic theory. A fully electromagnetic solution has not been obtained for the AC case. Such a solution is expected to be exceedingly complicated and would easily mask the effects of the shock which is the subject of this article. Fig. 4, on the other hand, gives a much clearer illustration of the order of magnitude of the shock-induced current, compared with the classical induced current according to RS. This comparison was made ignoring all space charge effects.

Fig. 4 allows us to draw the following inferences on the roles of the shock-induced current, in comparison with the classical induced current according to RS.

1) The shock-induced current is unlikely to further degrade the signal quality in satellite communication as a result of multipactor discharge. The underlying reason is that the multipactoring electrons typically have impact energies of order 100 eV or less [7], at which the shock-induced current has too small an effect to add significantly to the in-phase (I) and quadrature (Q) components of the signal errors [8]. Note that the I and Q components essentially represent the degree of beam loading on an RF circuit, and they are measured by the *area* under the induced current curves in Fig. 4 [8, Appendix B]. Thus, a low (high) electron impact energy such as 100 eV (340 keV) has a weak (strong) effect on beam loading, even though the peak values of the induced current are high in Fig. 4 at all impact energies.
2) Thus, the shock-induced current may provide appreciable beam loading to the RF circuits in those radiation sources in which the electrons impact the RF circuit with mildly relativistic energy, such as 340 keV ($\beta = 0.8$) in Fig. 4, in addition to the beam loading according to the preimpact, classical RS theory. A MILO and a relativistic magnetron may, therefore, suffer from appreciable beam loading due to this shock-induced current as the spoke electrons always strike the anode slow wave structure [12], [13].
3) Linear beam tubes, such as the traveling wave tubes and klystrons would not be affected as much by this shock-induced current because there is little beam interception in the interaction region.

One may wonder if the additional beam loading due to the electromagnetic shocks, as described in 2) for relativistic crossed-field devices, is one reason for the characteristically low efficiencies experienced in relativistic magnetrons (compared with microwave oven magnetrons) and in MILO experiments [14], [15].

IV. Concluding Remarks

In this article, we have isolated the effects of the electromagnetic shock phenomenon produced by the impact of a line charge on a conducting plate and evaluated the associated induced surface current. We have compared the induced current of this purely electromagnetic effect with the electrostatic induced current of a charge subject to an RF voltage in a parallel-plate geometry. This comparison was made only during one transit, which presumably gives an adequate assessment for steady-state operation in which one transit is essentially repeated each RF cycle. We have ignored all electromagnetic wave reflections, which necessarily occur in a parallel-plate geometry. This also is presumably adequate since the classical RS theory, which ignores all such reflections, is known to give a reasonably accurate value of the induced current in RF vacuum electronics, when there is little beam interception. The underlying reason for this unexpected feature has been explored [9].

We tentatively conclude that the shock-induced surface current will not cause additional damage in multipactor discharge, because of the low-impact energies of the multipactoring electrons. However, the shock-induced currents could be important in MILOs and relativistic magnetrons, in which spoke electrons, a significant fraction of which may have high energies (a few tens to hundreds of keV), always strike the anode circuit [14], [15]. The shock-induced current, in this case, would introduce additional beam loading that is omitted in the classical RS theory. This additional beam loading, leading to de-tuning and de-Q'ing of the circuit, is not easy to quantify. Here, we only note that they could be appreciable in MILOs and relativistic magnetrons. We suggest that this additional beam loading is unimportant for nonrelativistic crossed-field devices, consistent with our experience that the classical RS-induced current provides reasonably accurate results in computer simulations, when compared with measurements [5], [6].

APPENDIX A. DERIVATION OF (2)

With $vt' \equiv vt - h$, we write (1) as

$$K_x = \frac{\lambda\gamma^2 vx}{\pi[x^2+\gamma^2v^2t'^2]} \times \frac{ct+\frac{v^2t'-v^2t}{c}}{[(ct)^2-x^2-v^2t'^2-v^2t^2+2v^2tt']^{1/2}}. \quad \text{(A-1)}$$

We now take the limit $t \to \infty$ (and t' is finite) to get

$$\lim_{t\to\infty} K_x = \frac{\lambda\gamma^2 vx}{\pi[x^2+\gamma^2v^2t'^2]} \times \frac{c-\frac{v^2}{c}}{[c^2-v^2]^{1/2}} = \frac{\lambda\gamma vx}{\pi[x^2+\gamma^2v^2t'^2]}. \quad \text{(A-2)}$$

In terms of dimensionless quantities defined in the paragraph below (2), we may write

$$\bar{K}_x = \frac{\gamma\bar{x}}{\pi[\bar{x}^2+\gamma^2\bar{t}'^2]} \quad \text{(A-3)}$$

for $\bar{t}' < 0$.

APPENDIX B. DERIVATION OF (3)

Imposing the single-plate limit ($n = 0$) and $v \to -v$, we may write [9, eq. (14b)] as

$$\bar{K}_x = \mathbf{K}(\bar{x},-\bar{t},\bar{h}) - \mathbf{K}(\bar{x},-(\bar{t}-\bar{T}),0) = -\frac{\bar{x}(-\bar{t}/\beta+\bar{t}\beta-\bar{t}'\beta)}{\pi[(\bar{t}/\beta)^2-\bar{x}^2-\bar{t}'^2-\bar{t}^2+2\bar{t}\bar{t}']^{1/2}[\bar{t}'^2+\bar{x}^2/\gamma^2]} + \frac{\bar{x}(-\bar{t}'/\beta)}{\pi[(\bar{t}'/\beta)^2-\bar{x}^2]^{1/2}[\bar{t}'^2+\bar{x}^2/\gamma^2]} \quad \text{(B-1)}$$

where $t' = t - T$. Taking the limit of $t, T \to \infty$, while t' is finite, we obtain

$$\lim_{\bar{t}\to\infty} \bar{K}_x = -\frac{\bar{x}(-1/\beta+\beta)}{\pi[1/\beta^2-1]^{1/2}[\bar{t}'^2+\bar{x}^2/\gamma^2]} + \frac{\bar{x}(-\bar{t}'/\beta)}{\pi[(\bar{t}'/\beta)^2-\bar{x}^2]^{1/2}[\bar{t}'^2+\bar{x}^2/\gamma^2]} = \frac{\gamma\bar{x}}{\pi\left[\bar{x}^2+\gamma^2\bar{t}'^2\right]}\left\{1-\frac{\gamma\bar{t}'/\beta}{[(\bar{t}'/\beta)^2-\bar{x}^2]^{1/2}}\right\} \quad \text{(B-2)}$$

for $\bar{t}' \geq 0$, which is (3b). Equation (3a) is derived in (A-3).

APPENDIX C. PHASE-LOCKING CONDITION IN THE RELATIVISTIC REGIME

As in the nonrelativistic case, we ignore image charge effects. In addition, we assume that the electric field is $-\tilde{V}_{\mathrm{RF}}/d$ for simplicity. The relativistic force law reads

$$\frac{dp}{dt} = m\frac{d(\gamma\dot{z})}{dt} = \frac{e\tilde{V}_{RF}}{d}\sin(\omega t+\theta) \quad \text{(C-1)}$$

where $\gamma = (1-\dot{z}^2/c^2)^{-1/2}$. Integrating both sides, assuming $\dot{z}(t=0)=0$, we obtain

$$\gamma\dot{z} = \zeta(t) \equiv -\frac{e\tilde{V}_{\mathrm{RF}}}{m\omega d}(\cos(\omega t+\theta)-\cos\theta) \quad \text{(C-2)}$$

which may be rearranged to read

$$\dot{z} = \frac{dz}{dt} = \frac{\zeta(t)}{\left(1+\zeta^2(t)/c^2\right)^{1/2}}. \quad \text{(C-3)}$$

Integrating again, we obtain

$$z - d = \int_0^t dt\frac{\zeta(t)}{\left(1+\zeta^2(t)/c^2\right)^{1/2}}. \quad \text{(C-4)}$$

Since $z = 0$ when $\omega t = \pi$, (C-2) and (C-4) become

$$\zeta(t) = -\frac{e\tilde{V}_{\mathrm{RF}}}{m\omega d}(-\cos(\omega t)+1) \quad \text{(C-5)}$$

$$\int_0^{\pi/\omega} dt\frac{-\zeta(t)}{\left(1+\zeta^2(t)/c^2\right)^{1/2}} = d \quad \text{(C-6)}$$

where we have set the launch angle $\theta = \pi$. Equations (C-5) and (C-6) can be used to determine ω as a function of $\tilde{V}_{\mathrm{RF}}$, which is shown in the solid blue curve in Fig. 5. From (C-3) and (C-5), we may write the impact speed as

$$\beta = \frac{\frac{2e\tilde{V}_{\mathrm{RF}}}{mc\omega d}}{\left(1+\left(\frac{2e\tilde{V}_{\mathrm{RF}}}{mc\omega d}\right)^2\right)^{1/2}}. \quad \text{(C-7)}$$

Clearly, in the nonrelativistic limit, $c \to \infty$, $\beta = 2e\tilde{V}_{\mathrm{RF}}/mc\omega d$. This nonrelativistic limit and (C-7) are shown in the orange curves in Fig. 5.

ACKNOWLEDGMENT

The authors would like to thank Prof. Zhong He at the University of Michigan, Ann Arbor, MI, USA, for useful discussions.

REFERENCES

[1] S. Ramo, "Currents induced by electron motion," *Proc. IRE*, vol. 27, no. 9, pp. 584–585, Sep. 1939, doi: 10.1109/JRPROC.1939.228757.
[2] W. Shockley, "Currents to conductors induced by a moving point charge," *J. Appl. Phys.*, vol. 9, no. 10, pp. 635–636, 1938, doi: 10.1063/1.1710367.
[3] J. W. Gewartowski and H. A. Watson, *Principles of Electron Tubes: Including Grid-Controlled Tubes, Microwave Tubes, and Gas Tubes*. Princeton, NJ, USA: Van Nostrand, 1965.
[4] C. K. Birdsall and W. B. Bridges, *Electron Dynamics of Diode Regions*. New York, NY, USA: Academic, 1966.
[5] G. E. Dombrowski, "Simulation of magnetrons and crossed-field amplifiers," *IEEE Trans. Electron Devices*, vol. ED-35, no. 11, pp. 2060–2067, Nov. 1988, doi: 10.1109/16.7428.
[6] D. P. Chernin, "Computer simulations of low noise states in a high-power crossed-field amplifier," *IEEE Trans. Electron Devices*, vol. 43, no. 11, pp. 2004–2010, Nov. 1996, doi: 10.1109/16.543039.
[7] R. Kishek and Y. Y. Lau, "Interaction of multipactor discharge and RF circuit," *Phys. Rev. Lett.*, vol. 75, no. 6, pp. 1218–1221, Aug. 1995, doi: 10.1103/PhysRevLett.75.1218.
[8] P. Y. Wong, Y. Y. Lau, P. Zhang, N. Jordan, R. M. Gilgenbach, and J. Verboncoeur, "The effects of multipactor on the quality of a complex signal propagating in a transmission line," *Phys. Plasmas*, vol. 26, no. 11, Nov. 2019, Art. no. 112114, doi: 10.1063/1.5125408.
[9] D. Li, D. Chernin, and Y. Y. Lau, "A relativistic and electromagnetic correction to the Ramo–Shockley theorem," *IEEE Trans. Plasma Sci.*, vol. 49, no. 9, pp. 2661–2669, Sep. 2021, doi: 10.1109/TPS.2021.3099512.
[10] J. D. Jackson, *Classical Electrodynamics*, 3rd ed. Hoboken, NJ, USA: Wiley, 1999, Sec. 13.7.
[11] J. R. M. Vaughan, "Multipactor," *IEEE Trans. Electron Devices*, vol. ED-35, no. 7, pp. 1172–1180, Jul. 1988, doi: 10.1109/16.3387.
[12] J. Benford, J. A. Swegle, and E. Schamiloglu, *High Power Microwaves*. Boca Raton, FL, USA: CRC Press, 2015.

[13] R. J. Barker, N. C. Luhmann, J. H. Booske, and G. S. Nusinovich, *Modern Microwave and Millimeter Wave Power Electronics*. Piscataway, NJ, USA: IEEE Press, 2004.
[14] Y. Y. Lau *et al.*, "Explicit Brillouin flow solutions in magnetrons, magnetically insulated line oscillators, and radial magnetically insulated transmission lines," *IEEE Trans. Plasma Sci.*, vol. 49, no. 11, pp. 3418–3437, Nov. 2021, doi: 10.1109/TPS.2021.3092606.
[15] D. A. Packard *et al.*, "Theory, simulation, and experiments on a magnetically insulated line oscillator (MILO) at 10 kA, 240 kV near Hull cutoff condition," *Phys. Plasmas*, vol. 28, no. 12, Dec. 2021, Art. no. 123102, doi: 10.1063/5.0071455.

Dion Li (Student Member, IEEE) is currently pursuing the B.S.E degree in engineering physics with the University of Michigan, Ann Arbor, MI, USA.

His current research interests include theory, computation, and numerical modeling of electromagnetic phenomenon, plasma, and laser wakefield accelerators, crossed-field diodes, and magnetic reconnection.

Mr. Li received the Best Student Paper Award for his work on the Ramo–Shockley (RS) Theorem at the 2021 IEEE International Conference on Plasma Science (ICOPS), and at the 2021 Graduate Student Symposium, Michigan Institute for Plasma Science and Engineering (MIPSE), University of Michigan, Ann Arbor, where he also won the 2022 Henry Ford II Prize of the College of Engineering. In the Spring and Summer of 2022, he received two consecutive internships at the Princeton Plasma Physics Laboratory under the Department of Energy's Science Undergraduate Laboratory Internships (SULI).

Patrick Y. Wong (Member, IEEE) received the B.S.E., M.S.E., and Ph.D. degrees from the University of Michigan, Ann Arbor, MI, USA, in 2014, 2015, and 2018, respectively.

He was a Post-Doctoral Researcher with the Department of Electrical and Computer Engineering, Michigan State University, East Lansing, MI, USA. His current research interests include theoretical and computational modeling of beam–circuit interactions in high-power microwave devices including traveling-wave tubes, magnetrons, and multipactor.

David Chernin received the Ph.D. degree in applied mathematics from Harvard University, Cambridge, MA, USA, in 1976.

He has been with Leidos, Reston, VA, USA, and its predecessor company SAIC since 1984, where he has conducted research on beam–wave interactions and other topics in the physics of particle accelerators and vacuum electron devices.

Y. Y. Lau (Fellow, IEEE) received the B.S., M.S., and Ph.D. degrees in electrical engineering from the Massachusetts Institute of Technology, Cambridge, MA, USA, in 1968, 1970, and 1973, respectively.

Since 1992, he has been a Professor with the University of Michigan, Ann Arbor, MI, USA, where he is specialized in radio-frequency sources, heating, and discharge. He became an Emeritus Professor in 2022.

Dr. Lau was elected Fellow of the American Physical Society (APS) in 1986. He received the 1999 IEEE Plasma Science and Applications Award and the 2017 IEEE John R. Pierce Award for Excellence in Vacuum Electronics. He served three terms as an Associate Editor for *Physics of Plasmas* from 1994 to 2002.